Functional Heterogeneity of Photosystem II in Domain Specific Regions of the Thylakoid Membrane of Spinach (*Spinacia oleracea L.*)†

John Veerman,‡ Michael D. McConnell,‡ Sergei Vasil'ev,‡ Fikret Mamedov,§ Stenbjörn Styring,§ and Doug Bruce*,‡

Department of Biology, Brock University, St. Catharines, Ontario, L2S 3A1, Canada, and Department for Photochemistry and Molecular Science, Molecular Biomimetics, Uppsala University, Box 523, S-751 20, Uppsala, Sweden

Received September 21, 2006; Revised Manuscript Received January 17, 2007

ABSTRACT: A mild sonication and phase fractionation method has been used to isolate five regions of the thylakoid membrane in order to characterize the functional lateral heterogeneity of photosynthetic reaction centers and light harvesting complexes. Low-temperature fluorescence and absorbance spectra, absorbance cross-section measurements, and picosecond time-resolved fluorescence decay kinetics were used to determine the relative amounts of photosystem II (PSII) and photosystem I (PSI), to determine the relative PSII antenna size, and to characterize the excited-state dynamics of PSI and PSII in each fraction. Marked progressive increases in the proportion of PSI complexes were observed in the following sequence: grana core (BS), whole grana (B3), margins (MA), stroma lamellae (T3), and purified stromal fraction (Y100). PSII antenna size was drastically reduced in the margins of the grana stack and stroma lamellae fractions as compared to the grana. Picosecond time-resolved fluorescence decay kinetics of PSII were characterized by three exponential decay components in the grana fractions, and were found to have only two decay components with slower lifetimes in the stroma. Results are discussed in the framework of existing models of chloroplast thylakoid membrane lateral heterogeneity and the PSII repair cycle. Kinetic modeling of the PSII fluorescence decay kinetics revealed that PSII populations in the stroma and grana margin fractions possess much slower primary charge separation rates and decreased photosynthetic efficiency when compared to PSII populations in the grana stack.

In the process of oxygenic photosynthesis plants utilize light energy to split water into molecular oxygen, protons, and electrons and produce both ATP and NADPH for use in carbon fixation. This process requires photosystem I (PSI[1]) and photosystem II (PSII) operating in tandem.

PSI and PSII core complexes are large supramolecular pigment−protein complexes containing 96 and 35 chlorophyll *a* (Chl *a*) molecules (*1*, *2*) and (*3*, *4*), respectively. In higher plants both photosystems are associated with peripheral Chl *a* and Chl *b*-containing antenna complexes, known as light harvesting complex I (LHCI) and light harvesting complex II (LHCII). The PSII associated LHC family includes the Chl binding proteins, CP24, CP26, and CP29. The PSI core complex associates with four LHCI monomers, while two LHCII trimers and three monomers (CP24, CP26 and CP29) are coupled to each PSII core. The association of the auxiliary antennae with the PSI core complex has generated a model of PSI−LHCI with a total of 167 Chl molecules (*5*, *6*) and a Chl *a/b* ratio of about 9. The PSII−LHCII complex is characterized as possessing about 150 Chl molecules, with a Chl *a/b* ratio of about 2.5 (*7*, *8*). In addition to these basic structural units, higher plants produce variable amounts of additional LHCII serving to supplement the light harvesting capacity of each photosystem. These additional LHCII complexes can be dynamically reallocated between the two photosystems to optimize cooperation between them in a process denoted as state transitions, see ref *9* for review.

Photosynthetic membranes of chloroplasts consist of the appressed regions (grana stacks) and the unappressed regions (stroma lamellae). Grana stacks contain a preponderance of PSII and the stroma lamellae PSI (*10*−*12*). PSII populations localized in these two membrane areas are fundamentally different with respect to antenna size and photochemical activity. PSII complexes in the grana stack represent a highly active population with respect to donor and acceptor side electron transport, while those in the stroma lamellae have been observed to be relatively inactive (*13*−*15*).

A mild sonication and phase fractionation method has been developed to isolate several grana and stroma fractions (*13*, *14*, *16*); these membrane fractions are illustrated with respect to their location in chloroplast thylakoid membranes in Figure 1. Studies of these fractions have indicated that inactivation of PSII with respect to oxygen evolution and forward electron transfer from Q_A progressively increases with increasing distance from the grana core (*13*−*15*). Lateral heterogeneity

† This work was supported by a research grant from NSERC to D.B. Work in Sweden was supported by the Swedish Research Council and the Swedish Energy Agency (S.S. and F.M.).

* Corresponding author. E-mail: dbruce@brocku.ca. Fax: 905 688-1855. Phone: 905 688-5550 ext 3826.

‡ Brock University.

§ Uppsala University.

[1] Abbreviations: PS, photosystem; RC, reaction center; Chl, chlorophyll; P680, primary electron donor in photosystem II; Q_A, primary quinone electron acceptor in photosystem II; DAS, decay-associated spectrum; F_0, the minimal fluorescence level associated with photochemically active or "open" reaction centers with an oxidized primary quinone electron acceptor, Q_A; F_M, the maximal level of fluorescence associated with photochemically inactive or "closed" reaction centers with reduced primary quinone electron acceptor, Q_A.

10.1021/bi061964r CCC: $37.00
Published on Web 02/16/2007

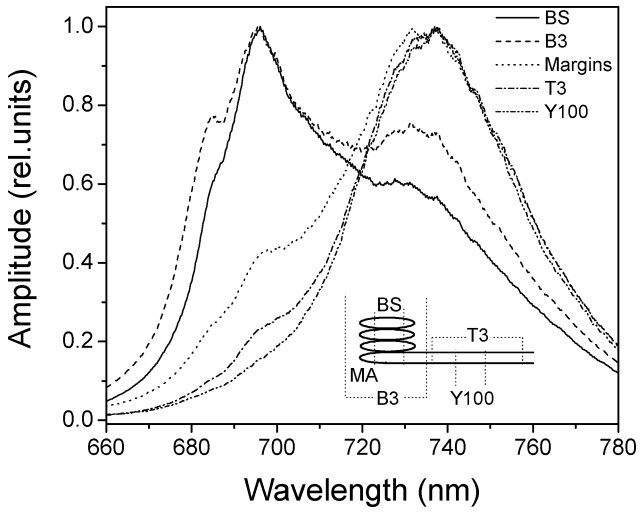

FIGURE 1: 77 K fluorescence spectra of chloroplast thylakoid fractions. Spectra were normalized to peak emission. BS, grana core fraction; B3, entire grana stack; margin, grana margins; T3, stroma thylakoid membranes; Y100, purified stroma thylakoid membranes. See Materials and Methods for details. Diagram illustrating the origin of the specific membrane fractions in relation to the structure of the chloroplast thylakoid membrane is shown in the inset.

of PSII was explained by damage of highly active PSII complexes in the grana core and their subsequent reallocation to the stroma membrane regions, which are accessible to ribosomes, for repair, see for review ref *17*. After repair in the stroma, Q_B binding affinity and the oxygen evolving complex were proposed to be restored during transport back to the grana. By the time PSII complexes reach the margins of the grana stack most are activated and the activation process was proposed to reach completion in the core of the grana stack (*13*, *14*). The isolation of thylakoid membrane fractions has allowed for the assessment of lateral heterogeneity with respect to Chl *a* and Chl *b* content, PSII/PSI ratio, and overall PSII activity as measured by secondary electron transport rates. In addition, the distribution of different forms of PSII, including PSII−LHCII supercomplexes, PSII dimers, PSII monomers, PSII monomers lacking CP43, and D1/D2 reaction centers, has been shown to vary greatly across fractions (*18*). The grana core contains most of the supercomplexes, and the PSII population in the Y100 fraction mostly consists of monomers lacking CP43 and D1/D2 reaction centers.

Characterization of primary energy conversion events in PSII, including excitation energy transfer, primary photochemical charge separation, charge stabilization, and recombination in the different thylakoid membrane fractions, has not yet been done. The rates of charge separation and stabilization can be obtained from picosecond time-resolved fluorescence decay kinetics. However, sophisticated kinetic modeling is required to estimate rates of photochemical processes in such complex pigment aggregates as PSI and PSII. Kinetic modeling, utilizing available structural information and assignment of site energy levels, has been applied to estimate rates of photochemical processes from fluorescence decay kinetics of isolated PSI and PSII particles (*2*, *19*−*22*). In the case of whole thylakoids many other factors (PSII heterogeneity, heterogeneity of the peripheral antenna, presence of unconnected light-harvesting complexes in the stroma lamellae, and mixing of PSI fluorescence with faster PSII decay processes) contribute to the complexity of the fluorescence decay kinetics, and determination of the intrinsic charge separation and charge stabilization rates becomes even more complex. Correct assignment of the observed fluorescence decay components is the first and the most critical step in the interpretation of fluorescence decay components in higher plant thylakoids.

Previously, fluorescence decay components of whole thylakoids have been assigned assuming that homogeneous PSI kinetics are monoexponential and PSII kinetics are biexponential (*23*, *24*). Two populations of PSII were required to fit data, and both populations were inferred to have two decay components with indistinguishable lifetimes of the fast decay components at F_0. The two populations were distinguished by finding a minimal physically reasonable kinetic model capable of describing a set of fluorescence decay kinetics measured at different wavelengths using samples with both closed (F_M) and open reaction centers. At F_M all four lifetimes could be distinguished and, as the relative amount of the two PSII populations was independent of the state of the reaction centers, it was possible to extract kinetic parameters of both PSII populations at F_0 by imposing this constraint on the fit of the F_0 kinetics.

Since then many studies have followed this assignment, particularly in interpretation of kinetic changes due to nonphotochemical quenching (*25*, *26*). Recent studies of isolated PSI and PSII particles have shown, however, that fluorescence decay kinetics of both photosystems are intrinsically more complex (*21*, *22*, *27*, *28*). Thylakoid membrane fractions isolated using the phase fractionation method represent simpler systems than whole thylakoids and are ideally suited for identification of fluorescence decay components. At the same time study of fluorescence decay kinetics in these fractions is critically important for understanding how the photochemical properties of PSII vary *in situ* in different thylakoid membrane regions and thus with different stages of the PSII repair cycle.

In this paper we present time-resolved fluorescence data, and measurements of the functional PSII antenna size of the aforementioned fractions of thylakoid membranes. We make use of independent measurements of relative PSI and PSII content, functional PSII antenna size, and global analysis of fluorescence decay kinetics collected with open and closed PSII reaction centers to identify decay components. Our data shows that the functional antenna size of PSII was drastically reduced in the margins of the grana stack and stroma fractions as compared to the grana. We found that fluorescence decay kinetics were relatively fast and three exponential in the grana fractions, while PSII in the stroma was characterized by slower and biexponential decay kinetics. Kinetic modeling of our data revealed essential differences in primary charge separation between PSII localized in the grana and stroma membrane regions. PSII primary charge separation rates and photosynthetic efficiency were depressed in the stroma derived fractions and the grana margins as compared to the grana stack. We discuss our results in the framework of the existing models of chloroplast thylakoid membrane structure and the PSII repair cycle.

MATERIALS AND METHODS

Preparation of Thylakoid Membrane Fractions. All thylakoid membrane fractions were isolated from home grown spinach as described in refs *14*, *15*.

Steady-State Spectroscopy. Absorption spectra were measured at 10 K using an intensified diode array detector (model 1461 EG&G Princeton Applied Research) and a helium cryostat (Advanced Research Systems, Inc., model DE-202). Samples were resuspended in 50 mM HEPES buffer, pH 7.6, containing 0.1 M sorbitol, 5 mM $MgCl_2$, 5 mM NaCl, and 60% glycerol. Emission spectra were measured at 77 K with the same detector. Chlorophyll concentration of less than 5 μg/mL was used in fluorescence measurements.

PSII Absorbance Cross Sections. PSII absorption cross sections were determined by flash saturation curves of variable Chl *a* fluorescence. An optical parametric oscillator (VisIR2, GWU-Lasertechnik) pumped by the third harmonics of a Q-switched Nd:YAG laser (Spectron Laser Systems) was used to provide 6 ns long actinic flashes at a wavelength of 435 nm. The actinic light was delivered via the optical fiber to a 250 μL flow through cuvette where the sample was circulated at the rate of about 1 mL/s. Chlorophyll concentration of about 5 μg/mL was used in cross-section measurements. Non-actinic 60 μs long measuring light pulses were supplied by blue light emitting diode (450 nm) 100 μs after the pump flash to determine the amplitude of fluorescence. Chlorophyll fluorescence was detected by a photomultiplier tube (Hamamatsu RG967), screened by a 1/4 m monochromator. A small fraction of the actinic flash was directed toward a photodiode so that the energy of each laser pulse could be measured. Twenty fluorescence yield and flash energy signals were averaged simultaneously at a flash frequency of 2.5 Hz. Data were fit with the cumulative Poisson single-hit probability distribution (*29*): $\Phi(I) = \Phi_{max}(1 - e^{-I\sigma})$ where I is the pulse energy, $\Phi(I)$ is the yield of the fluorescence, Φ_{max} is the maximal yield determined at saturating flash intensity, and σ is the effective absorption cross section.

Absorbance cross sections were also calculated based on the distribution of different types of PSII complexes found in the different fractions of the thylakoid membrane as reported by ref *18*. This was performed by representing each subpopulation of PSII with a cumulative Poisson single-hit probability distribution, taking into account the relative proportion and the presumed antenna size of the PSII subpopulation. For each fraction the cumulative Poisson single-hit probability distribution for each constituent subpopulation of PSII was added to produce a simulated curve. The simulation was then fit in the same manner as the experimentally obtained data. The relative antenna sizes of the various subpopulations of PSII identified in ref *18* (PSII−LHCII supercomplexes, PSII dimers, PSII monomers, CP43-less PSII monomers, and D1/D2 reaction centers) were calculated based on the following assumptions concerning the number of antenna Chl associated with each "type" of PSII. The D1/D2 reaction centers were assumed to contain the equivalent of 6 Chls, CP43-less centers had 22 Chls, and PSII monomers and PSII dimers possessed 35 Chls per reaction center (*30*). The PSII−LHCII supercomplexes were assumed to possess a variable number of Chls ranging from a minimum of 125 Chls to a maximum of 253 Chls per reaction center. The antenna size of PSII−LHCII was derived via use of CP24 (10 Chls), CP26 (9 Chls), and CP29 (8 Chls) monomeric subunits (*31*); and the LHCII trimers (42 Chls) (*32*) as the building blocks of the PSII auxiliary antennae. It should also be noted that the stroma derived fractions (margins, T3, and Y100) were assumed to possess PSII−LHCII complexes that were relatively disassembled when compared to the grana derived fractions (BS and B3); while PSII monomers and dimers in the grana derived fractions were assumed to possess some measure of auxiliary antennae. This disparity was mandated in order to determine if the PSII subpopulations were relatively more disassembled in the stroma as compared to the grana. The precise details regarding the implementation of this bias in our calculations can be found in the Results section.

Picosecond Fluorescence Decay Kinetics. A single photon timing apparatus utilizing a picosecond pulsed diode laser was used to measure the kinetics of chlorophyll fluorescence decays (*33*). Excitation pulses were delivered at 407 nm by a picosecond diode laser (PicoQuant, PDL 800-B), 54 ps fwhm. Chlorophyll fluorescence was measured by a Hamamatsu R-3809 micro channel plate photomultiplier screened by a double monochromator. A single photon counting PC card (Becker & Hickl, SPC-730) was used for data collection. The instrument response function of the system was 68 ps. To maintain PSII reaction centers in the open (F_0) state samples were circulated with a flow rate of 4 mL/s and low measuring light intensities were used. The F_M state was achieved by addition of DCMU, slowing down the circulation rate and increasing the measuring light intensity. Fluorescence decay data were collected for four detection wavelengths between 680 and 730 nm until 20 000 counts in the peak channel were attained. Fluorescence decay curves taken at all wavelengths were fit with the sum of exponential decay functions globally with the model of parallel decaying compartments as described previously (*34*, *35*).

PSII Kinetic Modeling. Modeling of PSII fluorescence decay kinetics was based on a recently published "coarse grained" model which takes into account supramolecular organization of PSII and LHCII in thylakoid membranes to model the energy migration and charge separation processes in the PSII−LHCII supercomplex (*22*). In this model each pigment−protein subunit in the PSII−LHCII supercomplex is represented by one compartment. The excitation transfer rate between all compartments was assumed to be $(17\ ps)^{-1}$, and charge separation in PSII was modeled by one reversible radical pair. The antenna size of the PSII population in each fraction was determined from the measured absorbance cross sections and analysis of protein gels, and the connectivity between antenna compartments was based on the structural organization of PSII−LHCII complexes. The fitting parameters in the model were the rate constant of charge separation (K_{CS}), its reversal (K_{CS}^{-}), and charge stabilization by secondary electron transfer to Q_A (K_{ST}). This model is approximate, however, it was demonstrated previously that it allows one to draw conclusions about the relative contributions of excitation energy transfer and charge separation to excited-state dynamics (*22*).

RESULTS

Low-Temperature Fluorescence Spectra. Low-temperature fluorescence emission spectra were measured to assay for

Table 1: PSII Absorbance Cross Sections Obtained from Flash Saturation Curves[a]

fraction	cross section		
	measured	calculated[b]	calculated[c]
BS	1	1	1
B3	0.9	0.91	0.9
Ma	0.31	0.43	0.29
T3	0.27	0.38	0.25
Y100	0.2	0.37	0.24

[a] The fit error is less than 5%. The calculated cross sections are based on biochemical data for the relative number of PSII supercomplexes, PSII cores, and CP43-less PSII cores found in each fraction in ref *18*. See text for details. All cross sections are expressed relative to the grana core fraction. [b] Cross sections based on the numbers of LHCII associated with PSII supercomplexes, dimers, and monomers in each of the fractions as determined by proteomic analysis in ref *18*. [c] Cross sections based on the same assumptions as above with the additional assumption that that all of the "free" LHCII trimers that were associated with the grana core fraction were energetically coupled to PSII−LHCII supercomplexes.

Table 2: Photochemical Rate Constants and Q_A Reduction Efficiency in Each Fraction as Determined via Kinetic Modeling

fraction	K_{CS}, ns^{-1}	ΔG,[a] cm^{-1}	K_{ST}, ns^{-1}	efficiency of charge stabilization,[b] %
BS	403	1036	2.82	92.8
B3	143	894	4.11	90.4
Ma	33.8	690	3.46	73.2
T3	13.1	807	3.06	65.6
Y100	7.7	597	1.7	49.6

[a] Free energy difference between the excited state of the RC and the radical pair was calculated from the forward and backward rates of electron transfer. [b] To characterize changes in efficiency of the reaction centers independently of the antenna size the number of pigments in the BS fraction was used for calculation in all fractions.

relative amounts of PSII and PSI in the thylakoid membrane fractions. The fluorescence peak at ~730 nm (F_{730}) arises from PSI, the fluorescence peak at ~695 nm (F_{695}) from PSII; while the fluorescence peak occurring at ~685 nm (F_{685}) originates in both PSII and LHCII. The F_{695}/F_{730} ratio is a reasonable indicator of the relative PSII/PSI ratio. The F_{695}/F_{730} ratio was high in the grana BS and B3 fractions. It sharply dropped in the margins, and decreased further in stroma fractions (Figure 1). The trend observed shows the amount of PSII decreasing from grana fractions to stroma fractions, while relative PSI content increases (Figure 1). This is consistent with existing models of PSII/PSI lateral heterogeneity in chloroplast thylakoid membranes and with EPR measurements performed on similar fractions (see Table 3) (*15*).

Low-Temperature Absorbance Spectra. Low-temperature absorbance spectra from the B3 and grana core BS regions are very similar to each other and are characterized by a peak in the Chl *a* Q_Y region at 676 nm for B3 and BS (Figure 2). Both fractions also exhibit a distinct short wavelength shoulder on the Qy band at 671 nm. These two spectra show a relatively large contribution from Chl *b* observed as a distinct peak at 650 nm. Absorption spectra from the T3 and Y100 stroma membrane fractions are characterized by significantly increased contributions of long wavelength Chl *a* forms of PSI to the Qy band. Increase of the abundance of these forms results in a red shift and broadening of the absorption peak in the Chl *a* Q_Y region. The contribution of Chl *b* to the absorption of these fractions (especially in the Y100 fraction) is much lower than in the grana fractions. The spectra from the grana margins are intermediate between the grana and stroma membrane fractions for all of the above-described characteristics. The absorption data follows the same trend as the emission data indicating that the amount of PSII and Chl *b* containing LHC complexes decreases from grana fractions to stroma fractions, while relative PSI content increases.

PSII Absorbance Cross Sections. The absorbance cross sections of the PSII complexes present in the thylakoid fractions were determined using pump probe fluorescence flash saturation curves as described in Materials and Methods. Analysis of the saturation curves showed the absorbance cross section of PSII to be the largest in the whole grana and grana core fractions and sharply decrease in the grana margins and stroma fractions (Table 1). There was a 3-fold reduction of the functional antenna size of the PSII complexes from the grana core fraction (BS) to the grana margins, and a 5-fold decrease from the BS fraction to the Y100 fraction. Since the amplitude of the Chl *b* peak in the absorbance spectra does not decrease proportionally to the decrease of the functional PSII antenna size, a dissociation of LHCII complexes from PSII in the grana margins and stroma fractions is likely responsible for much of the decrease in functional antenna size and is consistent with existing models of PSII repair and measurements of PSII heterogeneity in chloroplast thylakoid membranes (*18*).

The observed relative difference in PSII antenna size found between the different thylakoid membrane fractions was compared to calculated relative differences in antenna size that were based on a recent proteomic analysis of the thylakoid fractions (*18*). The proteomic analysis showed each isolated thylakoid fraction to have a unique heterogeneous population of PSII centers consisting of PSII−LHCII supercomplexes, PSII dimers, PSII monomers, CP43-less PSII monomers, and D1/D2 reaction centers. Our calculation assumed different antenna sizes for each of the different types of PSII centers, and two different analyses were done assuming variable sizes for the PSII−LHCII supercomplexes, see Materials and Methods for details. Both calculations assumed that PSII dimers and PSII monomers found in the margins, stroma, and Y100 fractions were not associated with any LHC's and that any PSII supercomplexes found in the margin fraction were associated with the equivalent of 3 LHCII trimers per PSII−LHCII supercomplex (125 Chls per reaction center). Both calculations also assumed that PSII dimers and PSII monomers in the grana core were associated with 2 LHCII trimers and 1 LHCII trimer respectively (106 Chls per reaction center). The only difference between the two calculations was the assumed size of the PSII−LHCII supercomplex in the grana core. The first calculation assumed that the PSII−LHCII supercomplexes found in the grana core were associated with the equivalent of 5 LHCII trimers per PSII−LHCII supercomplex (169 Chls per reaction center), which is the upper limit for size of an isolated PSII−LHCII supercomplex (*36*). The second calculation assumed that the PSII−LHCII supercomplexes in the core were associated with 9 LHCII trimers (253 Chls per reaction center). This assumption was based on previous studies that indicated a possible PSII antenna size of 250 Chls (*37*−*39*); provided that all the LHCII present in the grana were utilized by PSII.

Table 3: Characterization of the Different Fractions of the Thylakoid Membrane

fraction	Chl *a*/*b* (mol/mol)	O_2 evolution[a] [μmol of O_2/(mg of Chl)$^{-1}$ h^{-1}]	Chl/fraction,[b] %, ± 5	PSII/fraction,[b] %, ± 5	PSI/PSII[c]	Chl/$Y_D^{\bullet}$ [d]	Chl/P700^{+} [d] mol/mol
grana core	2.27	271	51	71	0.25 ± 0.06	355	1300
grana	2.60	240	64	81	0.43 ± 0.05	408	980
margins	3.62	94	13	10	1.28 ± 0.14	667	508
stroma	4.40	87	36	19	3.10 ± 0.11	971	316
Y100	7.51	0	5	1	12.7 ± 1.65	2780	222
thylakoids	3.11	127	100	100	1.13 ± 0.05	617	552

[a] Measured with 2 mM ferricyanide and 0.5 mM PpBQ as electron acceptor. [b] Calculated from the counter current distribution that provided the Chl yield in each fraction and from the EPR measurements for the PSII content in the different thylakoid fractions, data from ref *18*. [c] On the basis of EPR measurements, data from ref *15*. [d] On the basis of EPR measurements, data from ref *15*. Shows total number of Chl(*a*+*b*) molecules per PSII or PSI center. Note that not all these chlorophylls are connected to PSII or PSI (see discussion in ref *15* for explanation of the calculation of antenna size).

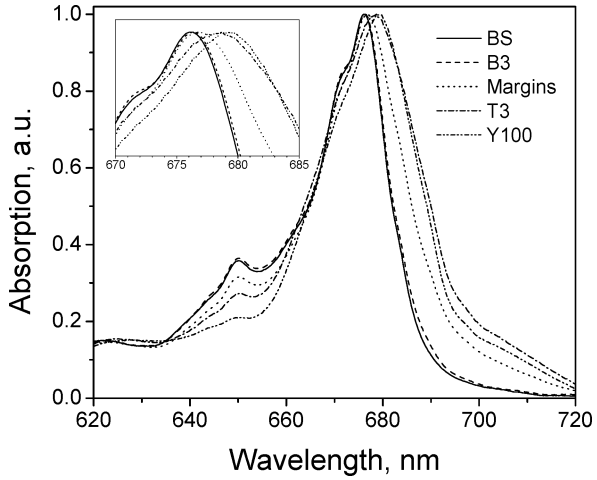

FIGURE 2: 10 K absorbance spectra of chloroplast thylakoid fractions. Spectra were normalized to peak absorbance. BS, grana core fraction; B3, entire grana stack; margin, grana margins; T3, stroma thylakoid membranes; Y100, purified stroma thylakoid membranes. Inset shows magnified picture of changes in the maximum absorption peak around 680 nm in the different fractions. See Materials and Methods for details.

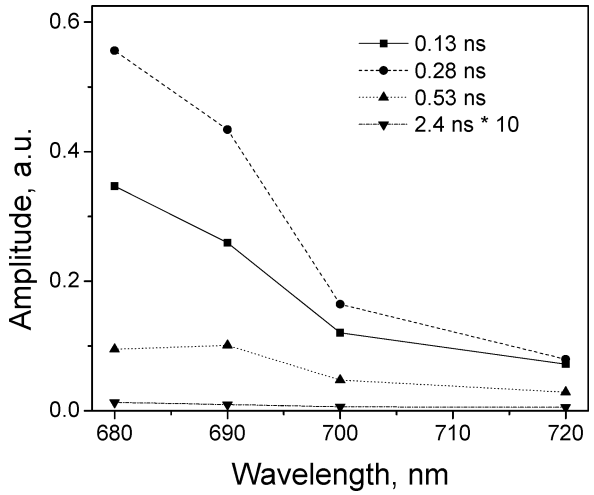

FIGURE 3: Decay-associated fluorescence emission spectra obtained from global analysis of picosecond fluorescent decay kinetics from the grana core fraction BS. See Materials and Methods for details.

In the first calculation, the assumptions used served to maximize the antenna size disparity between the grana fractions as compared to the margins, stroma, and Y100 by using the largest isolated PSII−LHCII antenna size as an upper limit (*37*−*39*) and the logical boundaries imposed by the PSII population distribution as reported previously in the proteomic data (*18*). Interestingly, in our first calculation, the relative PSII absorbance cross sections for the margins, stroma, and Y100 fractions were consistently higher than the experimentally determined cross sections (Table 1). The much larger antenna size for PSII−LHCII supercomplexes, that represented the only difference between the two calculations, generated relative absorbance cross sections which were much closer to the experimental results (Table 1).

Time-Resolved Fluorescence Decay kinetics. A global analysis of time-resolved fluorescence decay kinetics collected at both F_0 and F_M was undertaken to identify decay components originating from PSII and PSI. To facilitate the identification of the decay components we took advantage of the fact that PSI decay kinetics exhibit negligible changes between F_0 and F_M states. This allowed us to share the amplitudes and lifetimes of PSI components in simultaneous fits of data collected at both F_0 and F_M of the PSII reaction centers.

Since the best fits were obtained when the putative PSI components were linked in this manner, the assignment of components to PSII and PSI can be regarded as robust. It should also be noted that not only were the PSI components determined to be static from F_0 to F_M but these same components have been observed in isolated PSI-200 preparations (*40*, *41*) and the fast component has been also been observed in isolated PSI cores (*27*). In addition, as will be detailed in the following section, these assigned PSI components gradually emerge as the measurements move from grana to stroma; which is in accordance with our low-temperature fluorescence and absorbance measurements as well as a previous study of these fractions (*15*) and other grana and stroma preparations (*10*−*12*). We were particularly interested in characterization of fluorescence decay components originating from open PSII reaction centers as they reflect charge separation and charge stabilization processes.

The decay associated spectra for the grana core fraction BS are shown in Figure 3. Four components were required for the best possible fit of the data. Lifetimes of the three fastest decay components (τ_1 = 130 ps, τ_2 = 280 ps, and τ_3 = 530 ps) increased upon closure of PSII reaction centers (data not shown), and all of them had similar spectra. We assigned these components to open PSII reaction centers. The fourth minor component with the lifetime τ_4 = 2.4 ns was assumed to originate from a small fraction of closed PSII centers and/or uncoupled LHCII complexes. A similar

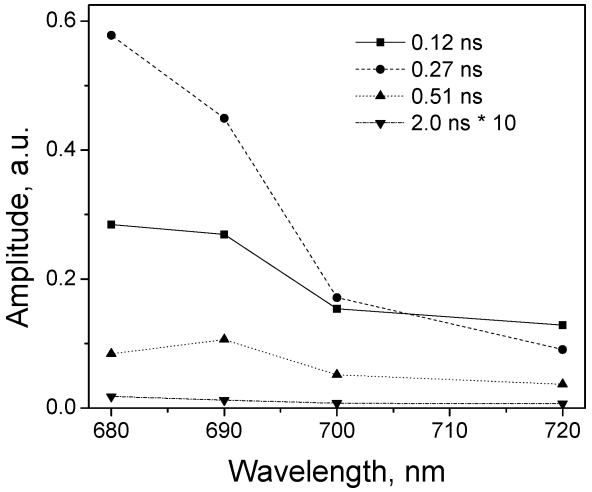

FIGURE 4: Decay-associated fluorescence emission spectra obtained from global analysis of picosecond fluorescent decay kinetics from the grana fraction B3. See Materials and Methods for details.

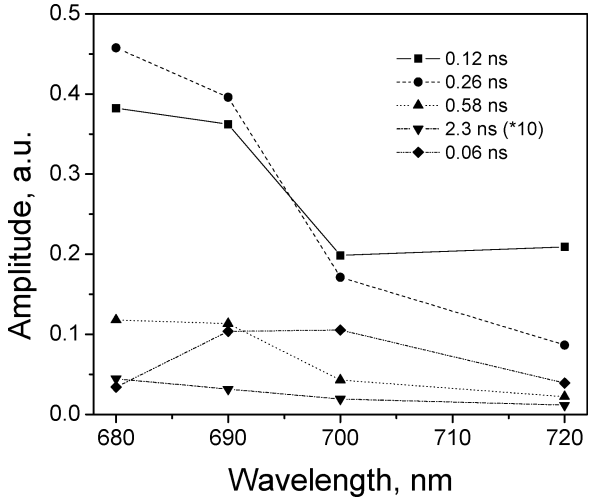

FIGURE 5: Decay-associated fluorescence emission spectra obtained from global analysis of picosecond fluorescent decay kinetics from the grana margin fraction.

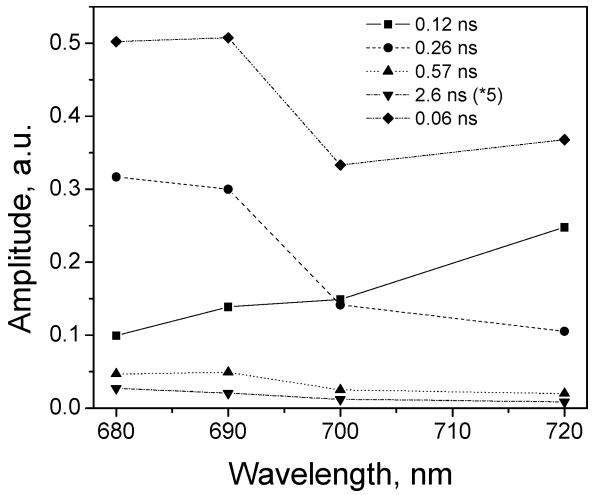

FIGURE 6: Decay-associated fluorescence emission spectra obtained from global analysis of picosecond fluorescent decay kinetics from the stroma thylakoid membrane fraction T3. See Materials and Methods for details.

component was observable in all of the fractions. Global analysis of the BS fraction generated decay associated spectra that lacked any identifiable PSI component, exemplifying the dearth of PSI complexes in the core of the grana stack.

Decay associated spectra of the whole grana (Figure 4) were quite similar to the grana core, with triphasic (τ_1 = 120 ps, τ_2 = 270 ps, and τ_3 = 510 ps) PSII kinetics and a minor τ_4 = 2.0 ns component. However, the shape of the spectra of the fastest decay component was altered when compared with the BS fraction. In the B3 fraction the 120 ps component showed an elevated amplitude at both 700 nm and particularly 720 nm. This indicated a contribution from PSI convolved with the fast component of PSII, attesting to a relative increase in the amount of PSI present when compared to the BS fraction. The contribution of PSI fluorescence to the fast decay phase was fairly small and virtually absent at wavelengths shorter than 700 nm. Decay kinetics of both grana fractions were found to be similar to the decay kinetics of BBY particles reported recently (*22*).

Fluorescence decay kinetics of the margins of grana stacks were more complex than the kinetics of grana fractions (Figure 5). Along with four components with lifetimes similar to corresponding components found in the grana fractions, an extra component with a lifetime τ_5 = 60 ps was required to describe the data. The amplitude and lifetime of this component were unaffected by the closure of PSII reaction centers, suggesting an origin in PSI. The red-shifted fluorescence emission peak of the 60 ps component was also indicative of PSI emission. A similar component was also observed in the decay kinetics of isolated PSI-200 particles (*40*). Thus, the 60 ps decay component of margins was assigned to PSI. This component was therefore shared and held constant in the global analysis of F_0 and F_M data. As was observed for grana fractions, the lifetimes of three of the decay components (τ_1 = 120 ps, τ_2 = 260 ps, and τ_3 = 580 ps) increased upon closure of PSII reaction centers (data not shown), indicating their origins in PSII. However, the spectral shape of the τ_1 = 120 ps component exhibited an even greater bias toward emission at 720 nm as compared to the B3 fraction, indicating that this PSII component is mixed with PSI emission. Considering the emergence of the 60 ps PSI component and the change in shape of the PSII fast component, the relative proportion of PSI complexes clearly increases in margins compared to the whole grana. The two slow components of PSII were also apparent (τ_2 = 260 ps and τ_3 = 580 ps), with τ_3 = 580 ps exhibiting a relatively increased amplitude as compared to the BS and B3 fractions. This indicates that the mean lifetime of PSII decay kinetics in the grana margins was slower than in the other grana fractions. The slow 2.3 ns component also showed a significantly larger amplitude in the margins than in either the BS or B3 fractions. This could be indicative of an increase in the amount of uncoupled antenna.

Five components were also required to fit fluorescence decay kinetics of the stroma T3 fraction, similar to the case of margins (Figure 6). Based on results from steady-state spectroscopy (Figure 1) we expected this fraction to contain more PSI reaction centers. As anticipated, the contribution of PSI to the fluorescence decay was larger, thus allowing us to identify two distinct PSI decay components with lifetimes τ_5 = 60 ps and τ_1 = 120 ps. The 120 ps component had a similar lifetime to the PSII fast component from the grana fractions, but its spectral shape was clearly indicative

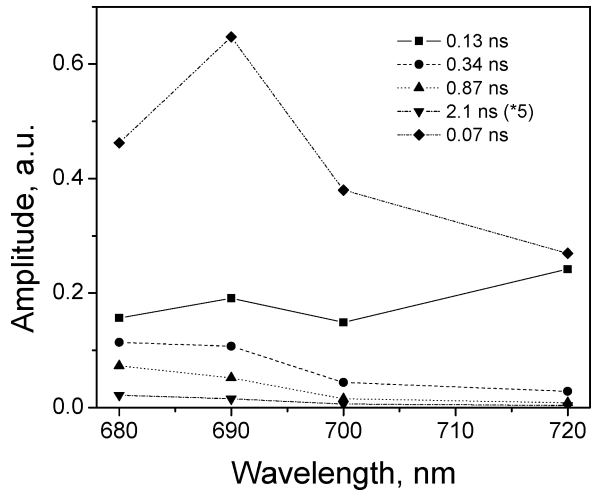

FIGURE 7: Decay-associated fluorescence emission spectra obtained from global analysis of picosecond fluorescent decay kinetics from the purified stroma fraction Y100. See Materials and Methods for details.

of PSI emission. Similar to what was observed for the 60 ps component, the 120 ps component showed no changes upon closure of PSII reaction centers. In our global analysis we, therefore, linked these two PSI components between the F_0 and F_M data sets through both amplitude and lifetime. Both the spectral shapes and relative amplitudes of the 60 ps and 120 ps components that emerged from fit of our data were very similar to the PSI decay components observed in isolated PSI−LHCI particles (*27*, *40*, *41*). The contribution of the PSI components confirmed an increased preponderance of PSI in the stroma lamellae as compared to the margins of the grana stack as seen in the fluorescence emission and absorption spectra (Figures 1, 2). The triphasic PSII decay kinetics observed in the grana fractions and grana margins were not present in the T3 stroma fraction. Only two decay components were found to be sensitive to trap closure, and they had lifetimes of 260 and 570 ps. Although a small amount of a fast 120 ps PSII component may have been mixed with the trap closure insensitive 120 ps PSI decay component, its relative amplitude, as compared to the two slow PSII decay kinetics, would be much smaller than that observed in the grana fractions. PSII decay kinetics are clearly different and much slower in the T3 stroma membrane fraction than in the grana or grana margin fractions. The contribution of the very slow 2.6 ns component to the fluorescence decay of T3 particles was larger than in grana fractions but similar to grana margins which may be indicative of more energetically uncoupled Chls in these regions.

The Y100 fraction, representing the purified stroma lamellae, showed the same two PSI components as observed in the T3 stroma lamellae (Figure 7). The spectral shapes, relative amplitudes, and lifetimes of these two components are very similar in both fractions and also to those previously determined in isolated PSI−LHCI particles (*27*, *40*, *41*). As found for the T3 fraction, the PSII decay kinetics in the Y100 fraction showed no evidence of a fast decay component. The two PSII associated decay components did, however, have even slower lifetimes, 340 ps and 870 ps. The very slow component was of similar amplitude to that observed in the T3 stroma lamellae. The Y100 fraction was thus characterized by significantly slower PSII decay kinetics as compared to the T3 fraction. The Y100 fraction also showed an increased contribution from PSI components, attesting to the increase in proportion of PSI complexes in the Y100 fraction. The analysis of this fraction completed the survey of PSI and PSII in the fractions, confirmed the increase in the PSI population, and revealed a slowing down of PSII kinetics when the sample origin moved from grana to stroma. In addition, the slower biphasic kinetics of PSII complexes in the stroma sharply contrasted with the triphasic kinetics in the grana supporting the idea of fundamentally different PSII populations in the grana as compared to the stroma with respect to charge separation and stabilization.

PSII Kinetic Modeling. The global analysis of the fluorescence decay kinetics revealed considerable differences in the decay components associated with PSII. Differences in PSII fluorescence decay kinetics can originate from different auxiliary PSII antennae and/or differences in the rates of charge separation in PSII. Early kinetic models for PSII assumed the kinetics to be dominated by trap limitation rather than transfer time from antenna to reaction center (*23*, *42*). Subsequent studies have shown that the migration time of excitation through the antenna complexes associated with PSII likely contribute to the overall fluorescent decay measured (*22*, *43*, *44*). Since the measured differences in PSII antenna size were considerable between the grana and stroma derived fractions, a recently introduced kinetic model (*22*), which could account for the antenna size differences, was used to model PSII decay kinetics.

The mean number of chlorophylls in the kinetic models for each PSII population was assigned as described above in the "PSII Absorbance Cross Sections" section. The resulting models are shown in Figure 8. In modeling of these "coarse-grained" representations of the PSII antenna system we assumed a uniform migration time of $(17\ \text{ps})^{-1}$ between all compartments. This value of intercompartment transfer time has been shown to describe BBY fluorescence decay kinetics within the context of this model (*22*) and is similar to the experimental value observed for excitation equilibration time in isolated LHCII trimers (*43*).

The kinetic model used in our study is approximate, and we do not expect to determine absolute values for charge separation rates with high accuracy. Nevertheless it is useful to compare results of our analysis of the kinetics with previous studies of isolated RC, PSII cores, and BBY particles. The rate of Q_A reduction in our fractions varies from $(243\ \text{ps})^{-1}$ in margins to $(590\ \text{ps})^{-1}$ in Y100. Holzwarth et al. (*45*). reported $(350\ \text{ps})^{-1}$ for PSII core complexes. We found the same value in the grana core fraction, Table 2. The free energy difference between the RC excited state and the radical pair is 1036 cm^{-1} for grana core fraction. Broess et al. (*22*) reported 2380 cm^{-1} for BBY preparations while in another study free energy difference between RC excited state and second radical pair was 930 cm^{-1} for PSII cores (*45*). Our estimation of the rate of charge separation in the grana core $(2.5\ \text{ps})^{-1}$ is between the rate determined in ref *22* for BBY preparations $(1.25\ \text{ps})^{-1}$ and the rate of charge separation determined by Holzwarth et al. (*45*) $(5.5\ \text{ps})^{-1}$ for PSII cores and isolated reactions centers. We have observed that when the size of antenna is close to the size of PSII antenna in the grana stack, the model becomes transfer to the trap limited, kinetics become insensitive to

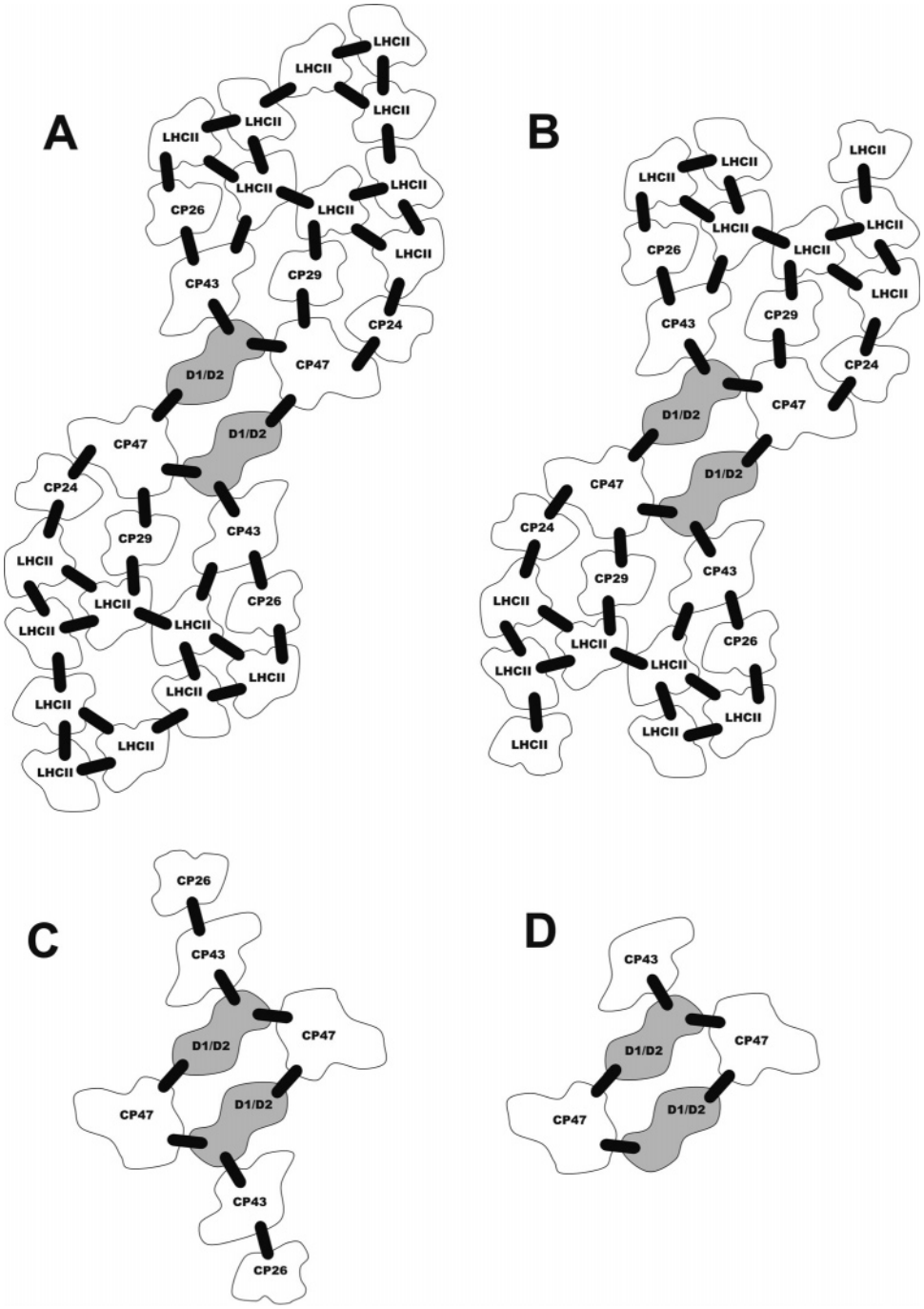

FIGURE 8: Schematic of PSII antenna size and connectivity between antenna compartments in the BS (A), B3 (B), margins (C), and T3/Y100(D) thylakoid fractions used in the kinetic model of PSII. Excitation transfer pathways are represented by the bars connecting compartments.

increase of K_{CS}, and alternative fits with higher K_{CS} are possible. Thus, our analysis of the grana core fraction representing active PSII revealed reasonable charge separation rates comparable with previous studies.

The rate constants for charge separation obtained by fitting fluorescence decay kinetics with the model are shown in Table 2. The results show a stark decrease in the rate of primary charge separation (K_{CS}) and photosynthetic yield characterizing the differences observed when moving from grana to stroma. The free energy difference between the excited state of RC and the radical pair also shows a similar trend while charge stabilization (K_{ST}) shows a modest relative increase in the margins, T3, and B3 fractions as compared to BS. This increase in K_{ST} may be attributable to alternate forms of electron transfer and will be dealt with in the discussion section in more detail.

The modeling results indicate that vast differences in PSII charge separation and by extension photosynthetic efficiency exist between the grana and stroma derived fractions. These results suggest that the grana core represents the only compartment in the thylakoid membrane with a highly functional PSII population, with the grana margins containing relatively inactive PSII while the stroma and Y100 fractions contain PSII populations that are severely limited with respect to charge separation. If the relative antenna size of each PSII population is considered, the margins of the grana stack and

stroma lamellae represent areas where the PSII population would provide a negligible contribution to overall photochemistry in the chloroplast.

DISCUSSION

Our low-temperature steady-state absorbance and fluorescence emission spectra are consistent with previous work describing the heterogeneous distribution of PSII and PSI within the thylakoid membrane (*11*, *14*, *46*). We found, as expected, a substantial increase in PSI associated long wavelength absorbance and emission peaks and decrease in PSII associated short wavelength absorbance and emission peaks in the T3 and Y100 stroma membrane regions as compared to the B3 and BS grana fractions. Absorbance and fluorescence spectra of the grana margins appeared to be intermediate in character between the spectra of grana and stroma membrane regions. These results are consistent with previous characterizations of the isolated fractions by room-temperature fluorescence induction, EPR spectroscopy, and pigment analysis (*13*, *14*)

We addressed the question of activity differences between PSII centers originating in different thylakoid regions by measuring the functional absorbance cross sections and picosecond fluorescence decay kinetics of the fractions. Our single turnover flash saturation measurements determine the functional absorbance cross section of PSII centers that are competent to undergo charge separation, reduce Q_A, and generate variable fluorescence. Our results show the PSII population in the whole grana and grana core fractions to have the largest absorbance cross sections. This is an expected result due to the clear association of PSII with LHCII in the grana (*7*, *9*, *47*, *48*). In contrast, PSII cross sections in the grana margins and stroma thylakoid membranes (T3 fraction) were considerably smaller. The decrease in functional antenna size in both margins and stroma regions was more than 3-fold compared to the grana core consistent with a large-scale dissociation of LHCII from PSII in the grana margins and in the stroma membrane regions. These results are consistent with recent models for PSII repair processes which propose the stripping off of LHCII as photodamaged PSII complexes leave the grana stacks for repair in the stroma membrane regions (*49*). However, when we attempted to model the decrease in antenna size of PSII between the grana core and margins and stroma membrane fractions based on recent proteomics data for the membrane fractions (*18*), it could not match the experimental result unless we assumed that the PSII−LHCII supercomplexes had a much larger antenna size (253 Chls per reaction center) than the largest isolated PSII−LHCII supercomplexes would be predicted to have (169 Chls per reaction center). A significant amount of "free" LHCII, existing as both trimers and monomers, is ubiquitous in nondenaturing gels of grana thylakoids (*48*, *49*), and a recent proteomic study of the different thylakoid membrane fractions also showed a significant amount of "free" LHCII in the grana core fraction as well as in the margin and stroma fractions (*18*). Early studies calculated an effective antenna size for PSII in the grana of approximately 253 Chls per reaction center based on the assumption that all of the LHCII present was energetically coupled to all of the PSII centers (*37*−*39*). Our absorbance cross section data is thus strong evidence that the "free" LHCII monomers and trimers observed in proteomic studies are functionally energetically connected to PSII in the grana cores, but not in the margins or stroma membrane regions.

The measured absorbance cross section of PSII in the Y100 fraction of the stroma lamellae was significantly smaller than for PSII in the margins or overall stroma membrane regions. This result was not predicted from the calculated absorbance cross sections based on the heterogeneity of PSII observed in the stroma and Y100 fractions (*18*). Until recently, the most highly disassembled type of PSII that could be observed using proteomics methods in the stroma lamellae had been identified as CP43-less PSII monomers (*48*, *49*). Recent work has shown that D1/D2 reaction centers are also found in stroma lamellae and Y100 fractions (*18*). The preponderance of disassembled PSII's (CP43-less PSII cores and PSII reaction centers) found in the Y100 fraction (*18*) is consistent with the idea that disassembly of the PSII core for purpose of repair may occur in the Y100 fraction. It has been previously shown that PSII repair specifically requires the removal of CP43 to allow access to the D1 protein subunit for removal and replacement (*48*); the physical reasons for this can be readily observed by considering the crystal structure of the PSII complex (*3*, *4*). Although additional patterns of PSII disassembly may occur during the repair cycle in order to facilitate the replacement of D2, psbH, CP47, CP43, and even the entire PSII complex via degradation and *de novo* synthesis, the majority of PSII repair involves D1 replacement (*48*, *50*). The smaller than expected cross section of PSII found in the Y100 fraction may arise from some form of additional excitation energy quenching in this fraction.

The PSII population in the core of the grana stack was characterized by triphasic fluorescence decay kinetics with lifetimes, relative amplitudes, and spectral shapes very similar to those of isolated BBY particles (*22*). There were no detectable PSI decay kinetics in this fraction. The grana margins exhibited noticeably slower PSII kinetics (larger contribution of slower decay components) as compared to the grana core and whole grana fractions. Slower PSII decay kinetics can result from increases in the antenna size as exemplified by recent model studies of PSII−LHCII (*22*). However, the PSII population in the margins had a much smaller antenna size than the PSII from the grana core so the slower decay kinetics must reflect changes in charge separation and/or stabilization in the PSII reaction center. Our data thus indicate a decline in the primary electron transport capability of PSII in the grana margins, a finding corroborated by a previous study showing that both donor and acceptor side electron transport in PSII are impaired in the margins of the grana stack (*14*). In the stroma derived fractions, the PSII-associated fast decay component is missing entirely and the remaining slow biphasic decay kinetics of PSII signify a drastic change in function, indicating a significant alteration of primary photochemistry. The slow biphasic decay we observe may be a characteristic of an over-riding mechanism responsible for inactivation of PSII in the stroma lamellae as part of the PSII repair process. Such an inactivation has been proposed to be due to disassembly of the manganese cluster (*13*, *14*), with eventual near total loss of the cluster in the Y100 fraction. Supporting this idea was the fact that the Y100 fraction exhibited even slower PSII decay kinetics than the stroma lamellae.

The differences observed in the kinetic modeling were pronounced; the difference between grana and stroma derived PSII populations K_{CS} was approximately 30 times, while a previous study on whole thylakoids determined the difference to be about 2.5 times (*23*). This disparity illustrates the utility of isolating fractions from each compartment, as the domination of the whole thylakoid PSII population by PSII originating in the grana core (Table 3) and the heterogeneity of PSII in whole thylakoids complicate the assignment of PSII components. In the case of the Y100 fraction, which only represents 1% of the total PSII population, observation of this compartment would be nearly impossible in whole thylakoids. In our measurements, the grana margins were the most complicated, due to the emergence of PSI components and the heterogeneity of the PSII population (*18*). As such, it should be noted that the modeling of the grana margins and to some extent the whole grana, which includes a considerable margin fraction, should be examined with some reservation. However, the rate constants and efficiency of the grana margins remain reasonable as previous studies show the compartment as containing a PSII population with intermediate electron-transfer facility (*13*, *14*). In the case of the stroma derived fractions, PSII assignment of decay components appears critical since the proportion of PSII decreases and the emergence of a possible PSII/PSI composite component in the 100 ps range. However, we did model this possibility in the Y100 fraction; a reasonable assignment of 20% of identified PSI components to PSII in our modeling yielded a K_{CS} of 23 and efficiency of 62%; while assigning all fast decay to PSII in the Y100 fraction yielded a K_{CS} of only 41 and an efficiency of 74%. Considering this, our assignment of a low amplitude fast component to PSI in the margins, although reasonable, had a nominal effect on the modeling results. As stated in the Results section, the K_{ST} was elevated in the B3, margins, and T3 as compared to the BS fraction. This increase in stabilization rate may represent the loss of excitation through unconventional channels, as the margins represent the beginning of PSII assembly and inactivation in the repair cycle (*13*, *14*).

In summary, our data shows that PSII centers capable of generating variable fluorescence are only functionally connected to peripheral antennae within the core of the grana stacks and primary electron transport is highly modified in PSII centers found in the stroma membrane regions. Specifically, decreased primary charge separation, decreased free energy difference between the excited state of the RC and the radical pair, and decreased overall photosynthetic efficiency characterize the PSII population in the grana margins and stroma lamellae. The heterogeneity in PSII absorbance cross sections and primary PSII activity of the thylakoid membrane fractions we observed supports existing models of compartmentalized PSII repair in chloroplast thylakoid membranes (*14*, *48*, *49*).

ACKNOWLEDGMENT

We gratefully acknowledge biochemical preparations by and discussions with Prof. Per-Åke Albertsson (Lund University), Dr. Ravi Danielsson (Lund University), and Dr. Rena Gadjieva (Swedish Agricultural University, Uppsala).

REFERENCES

1. Schubert, W.-D., Klukas, O., Krauss, N., Saenger, W., Fromme, P., and Witt, H.-T. (1997) Photosystem I of Synechococcus elongatus at 4 angstrom resolution: Comprehensive structure analysis, *J. Mol. Biol. 272*, 741−769.
2. Jordan, P., Fromme, P., Witt, H.-T., Klukas, O., Saenger, W., and Krass, N. (2001) Three-dimensional structure of cyanobacterial photosystem I at 2.5 Å resolution, *Nature 411*, 909−917.
3. Ferreira, K. N., Iverson, T. M., Maghlaoui, K., Barber, J., and Iwata, S. (2004) Architecture of the photosynthetic oxygen-evolving center, *Science 303*, 1831−1838.
4. Kern, J., Loll, B., Zouni, A., Saenger, W., Irrgang, K. D., and Biesiadka, J. (2005) Cyanobacterial Photosystem II at 3.2 angstrom resolution-the plastoquinone binding pockets, *Photosynth. Res. 84*, 153−159.
5. Ben Shem, A., Frolow, F., and Nelson, N. (2003) Crystal structure of plant photosystem I, *Nature 426*, 630−635.
6. Jolley, C., Ben Shem, A., Nelson, N., and Fromme, P. (2005) Structure of plant photosystem I revealed by theoretical modeling, *J. Biol. Chem. 280*, 33627−33636.
7. Nield, J., Orlova, E. V., Morris, E. P., Gowen, B., van Heel, M., and Barber, J. (2000) 3D map of the plant photosystem II supercomplex obtained by cryoelectron microscopy and single particle analysis, *Nat. Struct. Biol. 7*, 44−47.
8. Barber, J. (2002) Photosystem II: a multisubunit membrane protein that oxidises water, *Curr. Opin. Struct. Biol. 12*, 523−530.
9. Dekker, J. P., and Boekema, E. J. (2005) Supramolecular organization of thylakoid membrane proteins in green plants, *Biochim. Biophys. Acta−Bioenerg. 1706*, 12−39.
10. Anderson, J. M. (2002) Changing concepts about the distribution of Photosystems I and II between grana-appressed and stroma-exposed thylakoid membranes, *Photosynth. Res. 73*, 157−164.
11. Andersson, B., and Anderson, J. M. (1980) Lateral Heterogeneity in the Distribution of Chlorophyll-Protein Complexes of the Thylakoid Membranes of Spinach-Chloroplasts, *Biochim. Biophys. Acta 593*, 427−440.
12. Melis, A., and Anderson, J. M. (1983) Structural and functional organization of the photosystems in spinach chloroplasts. Antenna size, relative electron-transport capacity, and chlorophyll composition, *Biochim. Biophys. Acta 724*, 473−484.
13. Mamedov, F., and Styring, S. (2003) Logistics in the life cycle of Photosystem II-lateral movement in the thylakoid membrane and activation of electron transfer, *Physiol. Plant. 119*, 328−336.
14. Mamedov, F., Stefansson, H., Albertsson, P. A., and Styring, S. (2000) Photosystem II in different parts of the thylakoid membrane: A functional comparison between different domains, *Biochemistry 39*, 10478−10486.
15. Danielsson, R., Albertsson, P. A., Mamedov, F., and Styring, S. (2004) Quantification, of photosystem I and II in different parts of the thylakoid membrane from spinach, *Biochim. Biophys. Acta−Bioenerg. 1608*, 53−61.
16. Albertsson, P.-Å., Andréasson, E., Stefansson, H., and Wollenberger, L. (1986) Fractionation of thylakoid membrane, *Methods Enzymol. 228*, 469−482.
17. Kanervo, E., Suorsa, M., and Aro, E. M. (2005) Functional flexibility and acclimation of the thylakoid membrane, *Photochem. Photobiol. Sci. 4*, 1072−1080.
18. Danielsson, R., Suorsa, M., Paakkarinen, V., Albertsson, P. A., Styring, S., Aro, E. M., and Mamedov, F. (2006) Dimeric and monomeric organization of photosystem II-Distribution of five distinct complexes in the different domains of the thylakoid membrane, *J. Biol. Chem. 281*, 14241−14249.
19. Byrdin, M., Jordan, P., Krauss, N., Fromme, P., Stehlik, D., and Schlodder, E. (2002) Light harvesting in photosystem I: Modeling based on the 2.5-angstrom structure of photosystem I from Synechococcus elongates, *Biophys. J. 83*, 433−457.
20. Sener, M. K., Jolley, C., Ben Shem, A., Fromme, P., Nelson, N., Croce, R., and Schulten, K. (2005) Comparison of the light-harvesting networks of plant and cyanobacterial photosystem I, *Biophys. J. 89*, 1630−1642.
21. Miloslavina, Y., Szczepaniak, M., Muller, M. G., Sander, J., Nowaczyk, M., Rogner, M., and Holzwarth, A. R. (2006) Charge separation kinetics in intact photosystem II core particles is trap-limited. A picosecond fluorescence study, *Biochemistry 45*, 2436−2442.
22. Broess, K., Trinkunas, G., van der Weij-de Witt, C., Dekker, J. P., van Hoek, A., and van Amerongen, H. (2006) Excitation

energy transfer and charge separation in photosystem II membranes, *Biophys. J.* DOI: 10.1529/biophysj.106.085068.
23. Roelofs, T. A., Lee, C.-H., and Holzwarth, A. R. (1992) Global target analysis of picosecond chlorophyll fluorescence kinetics from pea chloroplasts, *Biophys. J. 61*, 1147−1163.
24. Holzwarth, A. R. and Roelofs, T. A. (1992) Recent advances in the understanding of chlorophyll excited- state dynamics in thylakoid membranes and isolated reaction center complexes, *J. Photochem. Photobiol. B—Biol. 15*, 45−62.
25. Wagner, B., Goss, R., Richter, M., Wild, A., and Holzwarth, A. R. (1996) Picosecond time-resolved study on the nature of high-energy-state quenching in isolated pea thylakoids-Different localization of zeaxanthin dependent and independent quenching mechanisms, *J. Photochem. Photobiol. B—Biol. 36*, 339−350.
26. Richter, M., Goss, R., Wagner, B., and Holzwarth, A. R. (1999) Characterization of the fast and slow reversible components of non-photochemical quenching in isolated pea thylakoids by picosecond time-resolved chlorophyll fluorescence analysis, *Biochemistry 38*, 12718−12726.
27. Croce, R., Dorra, D., Holzwarth, A. R., and Jennings, R. C. (2000) Fluorescence decay and spectral evolution in intact photosystem I of higher plants, *Biochemistry 39*, 6341−6348.
28. Vasil'ev, S., Lee, C.-I., Brudvig, G. W., and Bruce, D. (2002) Structure-based kinetic modeling of excited-state transfer and trapping in His-tagged PSII core complexes from *Synechocystis*, *Biochemistry 41*, 12236−12243.
29. Mauzerall, D., and Greenbaum, N. L. (1989) The absolute size of a photosynthetic unit, *Biochim. Biophys. Acta 974*, 119−140.
30. Loll, B., Kern, J., Saenger, W., Zouni, A., and Biesiadka, J. (2005) Towards complete cofactor arrangement in the 3.0 angstrom resolution structure of photosystem II, *Nature 438*, 1040−1044.
31. Sandona, D., Croce, R., Pagano, A., Crimi, M., and Bassi, R. (1998) Higher plants light harvesting proteins. Structure and function as revealed by mutation analysis of either protein or chromophore moieties, *Biochim. Biophys. Acta—Bioenerg. 1365*, 207−214.
32. Liu, Z. F., Yan, H. C., Wang, K. B., Kuang, T. Y., Zhang, J. P., Gui, L. L., An, X. M., and Chang, W. R. (2004) Crystal structure of spinach major light-harvesting complex at 2.72 angstrom resolution, *Nature 428*, 287−292.
33. Bruce, D., and Miners, J. (1993) Use of a pulsed laser diode to measure picosecond fluorescence lifetimes, *Photochem. Photobiol. 58*, 464−468.
34. Vasil'ev, S., Wiebe, S., and Bruce, D. (1998) Non-photochemical quenching of chlorophyll fluorescence in photosynthesis. 5-hydroxy-1,4-naphthoquinone in spinach thylakoids as a model for antenna based quenching mechanisms, *Biochim. Biophys. Acta 1363*, 147−156.
35. Vasil'ev, S., and Bruce, D. (1998) Nonphotochemical quenching of excitation energy in photosystem II. A picosecond time-resolved study of the low yield of chlorophyll a fluorescence induced by single-turnover flash in isolated spinach thylakoids, *Biochemistry 37*, 11046−11054.
36. Boekema, E. J., van Roon, H., Calkoen, F., Bassi, R., and Dekker, J. P. (1999) Multiple types of association of photosystem II and its light-harvesting antenna in partially solubilized photosystem II membranes, *Biochemistry 38*, 2233−2239.
37. Boekema, E. J., Hankamer, B., Bald, D., Kruip, J., Nield, J., Boonstra, A. F., Barber, J., and Rogner, M. (1995) Supramolecular Structure of the Photosystem-Ii Complex from Green Plants and Cyanobacteria, *Proc. Natl. Acad. Sci. U.S.A. 92*, 175−179.
38. Lam, E., Baltimore, B., Ortiz, W., Chollar, S., Melis, A., and Malkin, R. (1983) Characterization of A Resolved Oxygen-Evolving Photosystem-Ii Preparation from Spinach Thylakoids, *Biochim. Biophys. Acta 724*, 201−211.
39. Peter, G. F., and Thornber, J. P. (1991) Biochemical-Composition and Organization of Higher-Plant Photosystem-Ii Light-Harvesting Pigment-Proteins, *J. Biol. Chem. 266*, 16745−16754.
40. Ihalainen, J. A., Jensen, P. E., Haldrup, A., van Stokkum, I. H. M., van Grondelle, R., Scheller, H. V., and Dekker, J. P. (2002) Pigment organization and energy transfer dynamics in isolated, photosystem I (PSI) complexes from Arabidopsis thaliana depleted of the PSI-G, PSI-K, PSI-L, or PSI-N subunit, *Biophys. J. 83*, 2190−2201.
41. Melkozernov, A. N., Kargul, J., Lin, S., Barber, J., and Blankenship, R. E. (2004) Energy coupling in the PSI-LHCI supercomplex from the green alga Chlamydomonas reinhardtii, *J. Phys. Chem. B 108*, 10547−10555.
42. Dau, H., and Sauer, K. (1996) Exciton equilibration and photosystem II exciton dynamics—a fluorescence study on photosystem II membrane particles of spinach, *Biochim. Biophys. Acta 1273*, 175−190.
43. Barzda, V., Gulbinas, V., Kananavicius, R., Cervinskas, V., van Amerongen, H., van Grondelle, R., and Valkunas, L. (2001) Singlet-singlet annihilation kinetics in aggregates and trimers of LHCII, *Biophys. J. 80*, 2409−2421.
44. van Amerongen, H., and Dekker, J. P. Light-Harvesting in Photosystem II (2003) in *Light-Harvesting Antennas in Photosynthesis* (Green, B. R., and Parson, W. W., Eds.) pp 219−251, Kluwer Academic Publishers, Dordrecht.
45. Holzwarth, A. R., Muller, M. G., Reus, M., Nowaczyk, M., Sander, J., and Rogner, M. (2006) Kinetics and mechanism of electron transfer in intact photosystem II and in the isolated reaction center: Pheophytin is the primary electron acceptor, *Proc. Natl. Acad. Sci. U.S.A. 103*, 6895−6900.
46. Albertsson, P. A. (2001) A quantitative model of the domain structure of the photosynthetic membrane, *Trends Plant Sci. 6*, 349−354.
47. Kerfeld, C. A., Sawaya, M. R., Brahmandam, V., Cascio, D., Ho, K. K., Trevithick-Sutton, C. C., Krogmann, D. W., and Yeates, T. O. (2003) The crystal structure of a cyanobacterial water-soluble carotenoid binding protein, *Structure 11*, 55−65.
48. Aro, E. M., Suorsa, M., Rokka, A., Allahverdiyeva, Y., Paakkarinen, V., Saleem, A., Battchikova, N., and Rintamaki, E. (2005) Dynamics of photosystem II: a proteomic approach to thylakoid protein complexes, *J. Exp. Bot. 56*, 347−356.
49. Baena-Gonzalez, E., Barbato, R., and Aro, E. M. (1999) Role of phosphorylation in the repair cycle and oligomeric structure of photosystem II, *Planta 208*, 196−204.
50. Rokka, A., Suorsa, M., Saleem, A., Battchikova, N., and Aro, E. M. (2005) Synthesis and assembly of thylakoid protein complexes: multiple assembly steps of photosystem II, *Biochem. J. 388*, 159−168.

BI061964R